Journal of Cerebral Blood Flow & Metabolism (2012) 32, 264–277

www.jcbfm.com

JCBFM Open

The roles of cerebral blood flow, capillary transit time heterogeneity, and oxygen tension in brain oxygenation and metabolism

Sune N Jespersen[1] and Leif Østergaard[1,2]

[1]*Center of Functionally Integrative Neuroscience and MINDLab, NeuroCampus Aarhus, Aarhus University, Aarhus C, Denmark;* [2]*Department of Neuroradiology, Aarhus University Hospital, Aarhus C, Denmark*

Normal brain function depends critically on moment-to-moment regulation of oxygen supply by the bloodstream to meet changing metabolic needs. *Neurovascular coupling*, a range of mechanisms that converge on arterioles to adjust local cerebral blood flow (*CBF*), represents our current framework for understanding this regulation. We modeled the combined effects of *CBF* and capillary transit time heterogeneity (CTTH) on the maximum oxygen extraction fraction (OEF^{max}) and metabolic rate of oxygen that can biophysically be supported, for a given tissue oxygen tension. Red blood cell velocity recordings in rat brain support close hemodynamic–metabolic coupling by means of *CBF and* CTTH across a range of physiological conditions. The CTTH reduction improves tissue oxygenation by counteracting inherent reductions in OEF^{max} as *CBF* increases, and seemingly secures sufficient oxygenation during episodes of hyperemia resulting from cortical activation or hypoxemia. In hypoperfusion and states of blocked *CBF*, both lower oxygen tension and CTTH may secure tissue oxygenation. Our model predicts that disturbed capillary flows may cause a condition of *malignant* CTTH, in which states of higher *CBF* display *lower* oxygen availability. We propose that conditions with altered capillary morphology, such as amyloid, diabetic or hypertensive microangiopathy, and ischemia–reperfusion, may disturb CTTH and thereby flow-metabolism coupling and cerebral oxygen metabolism.
Journal of Cerebral Blood Flow & Metabolism (2012) **32,** 264–277; doi:10.1038/jcbfm.2011.153; published online 2 November 2011

Keywords: *CBF*; microcirculation; neurovascular coupling; oxygen transport; physiology

Introduction

Organs and tissues are generally believed to secure their supply of nutrients by adjusting arterial and arteriolar tone, and thereby local blood flow. Capillaries, in turn, bring blood in intimate contact with tissue, allowing diffusion of oxygen to nearby cells. Having demonstrated this diffusive transport, Danish physiologist August Krogh (1919) argued that capillaries themselves are part of the regulation of nutrient supply by *capillary recruitment*: opening of previously closed capillaries to increase the organ's total capillary surface area available for diffusion. In brain, capillary recruitment was ruled out after direct observation of red blood cell (RBC) transits through the capillary bed (Kuschinsky and Paulson, 1992); and consequently, *neurovascular coupling* (Roy and Sherrington, 1890)—mechanisms that adjust arteriolar tone according to local metabolic needs—represents our current framework for understanding the link between brain work and cerebral hemodynamics—and for interpreting human brain mapping studies using changes in blood oxygenation or cerebral blood flow (*CBF*)-related changes as proxies for neuronal activation.

Instead of temporary closing of capillaries, direct observations revealed extreme heterogeneity of RBC transit times across cerebral capillaries (Villringer *et al*, 1994; Pawlik *et al*, 1981), and stimulus-related changes in these flow patterns. The physiological significance of this phenomenon, and of the contractile *capillary pericyte*, the cell originally claimed to control capillary perfusion (Vimtrup, 1922), remains unclear. The contractile properties of pericytes have thus far been confirmed in brain capillaries and speculated to elicit upstream vasodilation (Peppiatt *et al*, 2006), but recent experiments suggest

Correspondence: Professor L Østergaard, Center of Functionally Integrative Neuroscience and MIND*Lab*, Building 10G, 5th Floor, Nørrebrogade 44, DK-8000 Aarhus C, Denmark.
E-mail: leif@cfin.dk
Both the authors were supported by the Danish National Research Foundation (CFIN) and the Danish Ministry of Science, Technology and Innovation's University Investment Grant (MIND*Lab*). LØ was supported by EU 6th framework IST program (I-Know).
Received 7 June 2011; revised 7 June 2011; accepted 30 September 2011; published online 2 November 2011

that functional hyperemia is controlled by arterioles independent of pericyte activity (Fernandez-Klett *et al*, 2010).

The development of quantitative neuroimaging techniques has revealed discrepancies between the changes in *CBF* and the corresponding changes in the cerebral metabolic rate of oxygen, $CMRO_2$, and hence the tissue oxygen extraction fraction (*OEF*). In normal brain, functional activation has, thus, been shown to result in *CBF* increases disproportionately larger than the increase in oxygen utilization as measured by positron emission tomography (Fox and Raichle, 1986). Elaborate modeling suggests that this apparent 'uncoupling' of oxygen consumption from the extent of functional hyperemia owes to biophysical limitations of oxygen diffusion from blood to tissue (Buxton and Frank, 1997; Hyder *et al*, 1998; Mintun *et al*, 2001; Zheng *et al*, 2002; Hayashi *et al*, 2003; Vafaee and Gjedde, 2000; Buxton, 2010; Davis *et al*, 1998). In particular, OEF decreases as *CBF* increases, highlighting a fundamental biophysical limitation of vasodilation as a means of meeting cellular demands for oxygen: as net oxygen delivery is proportional to $OEF \cdot CBF$, such reductions of *OEF* could substantially diminish the metabolic benefits of hyperemia.

Cellular oxygen metabolism itself facilitates oxygen extraction by producing more efficient blood-tissue concentration gradients. In states where *CBF* cannot increase, such as carotid stenosis, *OEF* is often increased without noticeable changes in *CBF* and cerebral blood volume (*CBV*) (Derdeyn *et al*, 2002). Recently, Leithner *et al* (2010) showed that oxidative brain metabolism in rats may proceed although *CBF* increases are largely blocked, confirming that 'isolated' *OEF* increase may be sufficient to drive the metabolism of activated neurons.

Studies of blood oxygenation in relation to cortical activity have further questioned *CBF*-metabolism coupling at the onset and cessation of neuronal activation: short-lasting blood deoxygenation (Malonek *et al*, 1997) at the onset of brain activation, and more consistent, prolonged poststimulus deoxygenation stages observed after episodes of cortical activation (Kruger *et al*, 1996), display *OEF* changes that seemingly cannot be explained by parallel changes in arteriolar tone (Donahue *et al*, 2009). The extent to which these phenomena represent 'true' uncoupling, during which oxidative metabolism proceed by increased extraction of capillary oxygen without parallel hemodynamic changes, or venular pooling of deoxygenated blood (Mandeville *et al*, 1999; Buxton *et al*, 1998), remains unclear.

In this paper, we examine the hypothesis originally proposed by Kuschinsky and Paulson (1992), namely that capillary flow patterns may affect the efficacy of oxygen extraction, even in the absence of 'true' recruitment. In rat, neural activation (Kleinfeld *et al*, 1998; Stefanovic *et al*, 2008; Schulte *et al*, 2003) and hypoxia (Krolo and Hudetz, 2000; Hudetz *et al*, 1997) are accompanied not only by increased flux of RBCs (owing to higher *CBF*), but also by rapid redistributions of capillary flows to more homogenous flow patterns. Such homogenization of capillary flow patterns has been pointed out to increase oxygen extraction efficacy (Østergaard *et al*, 2000), suggesting a mechanism by which OEF^{max} may change, independently of *CBF*.

Here, we extend existing compartment models, which describe the relation between net oxygen extraction, *CBF* and *CBV* (Buxton and Frank, 1997; Hyder *et al*, 1998; Mintun *et al*, 2001; Zheng *et al*, 2002; Hayashi *et al*, 2003; Vafaee and Gjedde, 2000; Buxton, 2010; Davis *et al*, 1998) to also take into account capillary transit time heterogeneity (CTTH) and tissue oxygen tension. Using data from *in-vivo* rat studies, we then compare the extent to which vasodilation, capillary transit time homogenization, and increased extraction of capillary oxygen (i.e., by increased blood-tissue pO_2 gradient alone) ensures cerebral oxygenation across a range of physiological conditions.

Materials and methods

Modeling Oxygen Extraction Capacity as a Function of Tissue Oxygen Tension and Capillary Transit Time Characteristics in Steady State

To incorporate the effect of CTTH on the upper biophysical limit for the proportion of oxygen that may be extracted by tissue, OEF^{max}, and hence the upper limit on the $CMRO_2$ that can be supported, $CMRO_2^{max}$, we first model the dependence of oxygen extraction from a single capillary $Q(\tau)$ on transit time τ, and then compute OEF^{max} and $CMRO_2^{max}$ by integrating over the distribution $h(\tau)$ of transit times in the capillary bed. Figure 1 presents an overview of the model in terms of the three parts involved: (1) a single capillary model of oxygen extraction $Q(\tau)$ as a function of transit time τ, (2) a description of capillary transit time distribution $h(\tau)$, and (3) the net extraction OEF^{max} from a capillary bed obtained by summing the single capillary contributions weighted by the transit time distribution,

$$OEF^{max} = \int_0^\infty d\tau\, h(\tau) Q(\tau) \tag{1}$$

The upper limit on $CMRO_2$ is then $CMRO_2^{max} = CBF \cdot C_A \cdot OEF^{max}$, where C_A is arterial oxygen concentration. We parameterize the probability density function of capillary transit times $h(\tau)$ by a gamma variate with parameters α and β.

$$h(\tau;\alpha,\beta) = \frac{1}{\beta^\alpha \Gamma(\alpha)} \tau^{\alpha-1} e^{-\tau/\beta} \tag{2}$$

The vascular mean transit time μ is then determined as $\alpha\beta$, and its standard deviation $\sigma = \sqrt{\alpha}\beta$ quantifies the heterogeneity of transit times among parallel capillary paths.

In modeling $Q(\tau)$, the oxygen extraction from a single capillary with transit time τ, we consider a three compartment model consisting of tissue, blood plasma, and hemoglobin. We assign the capillary length L and volume V, and assume that the current of oxygen across the

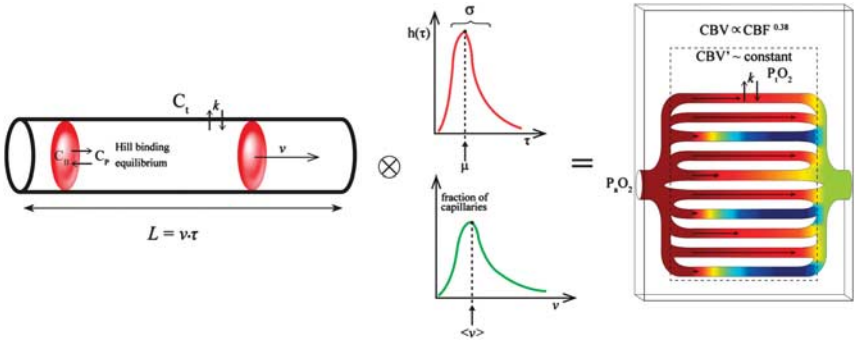

Figure 1 Model overview. On the left, the single capillary model is sketched. It consists of three compartments, oxygen bound to hemoglobin, oxygen in plasma, and oxygen in tissue. Oxygen in plasma is assumed to be in equilibrium with oxygen bound to hemoglobin, their concentrations related by the Hill equation. Transfer of oxygen across the capillary membrane is modeled as a first-order exchange process with the rate constant *k*. The capillary has a length *L*, and blood moves with a velocity *v* resulting in transit time $\tau = L/v$. The capillary bed on the right is then obtained as a collection of capillaries modeled as described, but with different transit times τ taken from the transit time distribution $h(\tau)$, as shown in the middle. Total capillary volume *CBV′* was assumed to either remain constant, or to vary with CBF in the same way as total blood volume, modeled here by Grubb's relation. CBF, cerebral blood flow; CBV, cerebral blood volume; *CBV′*, capillary blood volume.

capillary membrane is proportional to the difference between plasma oxygen concentration (C_p) and tissue oxygen concentration (C_t) (Mintun *et al*, 2001; Hayashi *et al*, 2003). The differential equation for total oxygen concentration C as a function of the fractional distance $x \in [0, 1]$ along the capillary with flow f and volume V then reads

$$\frac{dC}{dx} = -\frac{kV}{f}(C_p - C_t) \tag{3}$$

assuming steady state ($\partial C/\partial t = \partial C_t/\partial t = 0$), and equal forward and reverse rate constants k. Note that the capillary transit time τ is identical to V/f. The cooperativity of oxygen binding to hemoglobin is approximated by the phenomenological Hill equation:

$$C_B = B\frac{P^h}{P_{50}^h + P^h} \tag{4}$$

where C_B is the concentration of bound oxygen, B is the maximum amount of oxygen bound to hemoglobin, P is oxygen partial pressure in plasma, P_{50} is the oxygen pressure required for half saturation, and h is the Hill coefficient. Oxygen in the plasma is hence assumed to be in chemical equilibrium with oxygen bound to hemoglobin. Neglecting the contribution of plasma oxygen to the total oxygen content ($C_B \approx C$), we use equation (4) to express the oxygen pressure in terms of total oxygen content, and end up with a general equation for oxygen concentration as a function of the normalized distance x along a capillary with transit time τ (Mintun *et al*, 2001; Hayashi *et al*, 2003):

$$\frac{dC}{dx} = -k\tau\left(\alpha_H P_{50}\left(\frac{C}{B-C}\right)^{1/h} - C_t\right) \tag{5}$$

where α_H is Henry's constant. The model constants were assigned generally accepted literature values: $h = 2.8$, $B = 0.1943$ mL/mL, $C_A = 0.95 \cdot B$, $\alpha_H = 3.1 \times 10^{-5}$ per mm Hg, and $P_{50} = 26$ mm Hg (Hayashi *et al*, 2003). The equation can then be solved for x as a function of C (i.e., the inverse of C), when tissue oxygen concentration C_t is 0:

$$\alpha_H P_{50} k\tau x + C(x)^{1-1/h} B^{1/h} {}_2F_1\left(1 - 1/h,\ -1/h,\ 2 - 1/h;\ \frac{C(x)}{B}\right) / (1 - 1/h) = \text{constant} \tag{6}$$

The constant on the right-hand side is determined by the initial value, $C(0) = C_A$ and ${}_2F_1$ is a hypergeometric function. If oxygen binding cooperativity is ignored (in addition to the condition $C_t = 0$) so that $C_p \propto C$, capillary oxygen concentration will be given by the familiar exponential Crone-Renkin expression $C(x) = C(0) \cdot \exp(-k\tau x)$.

For an arbitrary but constant tissue oxygen tension C_t, we numerically solve the differential equation (5) to yield the single capillary extraction fraction $Q = 1 - C(1)/C(0)$ as a function of $k\tau$. The fact that Q depends on the product $k\tau$, and not on k and τ individually, allows us to estimate the OEF^{max} as a function of α, $k\beta$, and tissue oxygen tension, via

$$\begin{aligned} OEF^{max} &= \int_0^\infty d\tau \frac{1}{\beta^\alpha \Gamma(\alpha)} \tau^{\alpha-1} e^{-\tau/\beta} Q(k\tau) \\ &= \int_0^\infty dy \frac{1}{(k\beta)^\alpha \Gamma(\alpha)} y^{\alpha-1} e^{-y/(k\beta)} Q(y) \end{aligned} \tag{7}$$

For a steady-state condition characterized by C_t, μ, and σ, this procedure yields OEF^{max} by standard numerical integration techniques, with k as the only unknown parameter. The model constant k was fixed to yield resting $OEF^{max} = 0.3$ based on transit time data recorded by Stefanovic *et al* (2008) during forepaw stimulation in a rat (their Figures 3C and 3D). Consequently, k was set to $k = 118$ per second throughout the study.

Choice of Blood Volume Term for Maximum Cerebral Metabolic Rate of Oxygen Calculations

To determine $CMRO_2^{max}$ as a function of τ, *CBF* in the expression $CMRO_2^{max} = C_A \cdot CBF \cdot OEF^{max}$ must be replaced by CBV/τ, utilizing the central volume theorem (Stewart,

1894), while keeping in mind that τ and hence *CBV* applies only to the portion of the vasculature that allows exchange of oxygen with tissue. Although most vessel walls are known to be permeable to oxygen, most oxygen diffusion to cells is believed to originate from nearby capillaries rather than the much more distant, larger vessels (Pittman, 2011). We, therefore, used the capillary blood volume, *CBV′*, throughout our calculations. Capillary volume, in turn, may vary with *CBF*. We examined two extremes, namely (1) constant *CBV′* (i.e., higher *CBF* is paralleled by shorter transit time) and (2) the empirical *CBF–CBV′* relation based on *total* blood volume, as observed by positron emission tomography in brain (Grubb *et al*, 1974; see Figure 1). Where needed, rat *CBF* in the resting state was inferred from the central volume theorem based on the value of μ and $CBV' = 1.6\%$, resulting in a value of $CBF = 60$ mL/100 mL per minute. Arterial oxygenation was set to $C_A = 19$ mL/100 mL.

Analysis of Literature Transit Time Characteristics

Transit time distribution data were obtained from seven studies performed in rat (N = number of animals per group), including *cortical electrical stimulation* (control and 1.0 to 5.0 mA, $N = 6$ by Schulte *et al,* 2003, their Figure 5), *mild* (control and PaO_2 40 mm Hg, $N = 5$ by Hudetz *et al,* 1997, their Figure 2A) *and severe* (PaO_2 26 mm Hg, $N = 5$ by Krolo and Hudetz, 2000, their Figure 3) *acute hypoxia*, *graded hemorrhagic hypotension* (cerebral perfusion pressure 30 to 110 mm Hg, $N = 6$ by Hudetz *et al,* 1995, their Figure 4, assuming a gamma variate distribution of transit times), and *mild* (control and $PaCO_2$ 50 mm Hg, $N = 6$ by Villringer *et al,* 1994, their Figure 4) *and severe hypercapnia* (control and $PaCO_2$ at 67 and 97 mm Hg, $N = 5$, by Hudetz *et al,* 1997, their Figures 2B and 2C). Reported RBC velocity (v) distributions were converted to transit time (τ) distributions assuming $\tau = L/v$, where L/v is the length of the capillary path along which RBCs exchange oxygen with tissue before blood converges to draining venules. For $CBV' = 1.6\%$ and $CBF = 60$ mL/100 mL per minute (see above), the capillary mean blood transit time is $\tau = 1.6$ seconds. Measured resting RBC velocities are typically 0.25 to 1.5 mm/s (Kleinfeld *et al*, 1998), and we chose $L = 400\ \mu$m as a conservative estimate of this length. The assumption of a uniform capillary path length is discussed further below. For the hypercapnia study by Villringer *et al* (1994), the distribution of blood cell fluxes (n) during normocapnia and hypercapnia was read off from their Figure 4. An average RBC linear density $\langle \rho \rangle$ in the two conditions was then estimated by the ratios of the average cell fluxes $\langle n \rangle$ and the average blood cell speeds $\langle v \rangle$: $\langle \rho \rangle = \langle n \rangle / \langle v \rangle$. Note, this rough estimate is likely less certain than the approaches above. Finally, the distribution of blood cell fluxes was converted into a transit time distribution from the relation $\tau = L\langle \rho \rangle / n$.

To illustrate the relative importance of CTTH changes, $CMRO_2^{max}$ values were also given for the case in which CTTH was kept constant at its resting value (Table 1, rightmost column).

Choice of Literature Tissue Oxygen Tension Values

The measurement of tissue oxygen tension values ($P_t = C_t/\alpha_H$) in tissue is faced by a range of methodological challenges, and reports vary greatly in terms of absolute values and changes in response to physiological challenges (Ndubuizu and LaManna, 2007). We chose a resting tissue oxygen tension value of 25 mm Hg and chose per-stimulus values to reflect the generally accepted notion that tissue oxygen tensions tend to follow *CBF* changes (except during hypoxemic hyperemia). For hypercapnia and functional hyperemia, we thus interpolated relative to an oxygen tension increase of 5 mm Hg at maximum stimulation, and for hypotension and hypoxemia according to an oxygen tension drop of 8 mm Hg at minimum perfusion pressure and arterial oxygen tension, respectively. All oxygen tension values used in the model calculations are listed in Table 1. To illustrate the effects of tissue oxygen tension changes, all oxygen availability values were also reported for unaltered tissue oxygen tension (in parenthesis).

Results

Qualitative Analysis

We begin with a qualitative analysis of some of the effects of CTTH on oxygen extraction capacity. For simplicity, we consider tissue oxygen tension to be zero in this section.

Nonnegligible capillary transit time heterogeneity reduces maximum oxygen extraction fraction relative to single transit time kinetics: Figure 2A shows OEF^{max} as a function of the capillary transit time τ using the Crone-Renkin formula (Crone, 1963). Note that the function is concave and approaches zero as capillary transit times become very short. The dashed arrows represent two populations of capillaries with different transit times $\tau_1 < \tau_2$. The asterisk marks the resulting reduction in OEF^{max} relative to the case of a single transit time. Note that due to the concave shape of this relation, any CTTH among capillaries organized in parallel result in a reduction of OEF^{max}.

The parallel arrangement of capillaries allows maximum cerebral metabolic rate of oxygen to decrease with cerebral blood flow: Figure 2B shows the $CMRO_2^{max}$ curve as a function of tissue blood flow f. Considering only a single capillary, the net oxygen extraction capacity is always an increasing function of flow (in this case, f equals macroscopic *CBF*): OEF^{max} decreases with *CBF* at a rate that is slower than linear, and $CMRO_2^{max} = C_A \cdot OEF^{max} \cdot CBF$ is, therefore, always an increasing function of *CBF*. The slope of the curve, and hence the 'metabolic benefits' of hyperemia, however, decreases monotonically toward high *CBF*. This property changes in a population of capillaries: consider for simplicity, a system with fixed tissue oxygen tension and two populations of capillary paths having flow f_1 and f_2.

Table 1 *In-vivo* transit time characteristics during a range of physiological stimuli, estimated from literature RBC velocity data (references given in parenthesis)

	μ *(seconds)*	σ *(seconds)*	P_t *(mm Hg)*	*Model* OEF^{max}	$CMRO_2^{max}$ *Relative to control*	
					Model	*Constant CTTH*
Functional activation (N = 1) (*Stefanovic et al, 2008*)						
Control (0)	1.4	1.33	25	0.3	1.00	1.00
Activation (I)	0.81	0.52	30 (25)	0.22 (0.26)	1.25 (1.50)	0.85 (1.05)
Cortical electrical stimulation (N = 6) (*Schulte et al, 2003*)						
Control (0)	1.49	0.92	25	0.34	1.00	1.00
1.0 mA (I)	1.71	1.20	26 (25)	0.34 (0.35)	0.85 (0.89)	0.90 (0.94)
2.0 mA (II)	1.14	0.74	27 (25)	0.28 (0.31)	1.08 (1.17)	1.03 (1.11)
3.0 mA (III)	0.96	0.55	28 (25)	0.26 (0.29)	1.17 (1.31)	1.04 (1.17)
4.0 mA (IV)	0.62	0.32	29 (25)	0.20 (0.23)	1.43 (1.64)	1.04 (1.21)
5.0 mA (V)	0.63	0.23	30 (25)	0.21 (0.24)	1.41 (1.64)	1.00 (1.21)
Hypotension (N = 6) (*Hudetz et al, 1995*)						
115 mm Hg (0)	0.30	0.10	25	0.16	1.00	1.00
90 mm Hg (I)	0.31	0.11	24 (25)	0.16 (0.16)	1.02 (0.99)	1.02 (1.00)
75 mm Hg (II)	0.34	0.15	22 (25)	0.18 (0.17)	1.02 (0.94)	1.04 (0.96)
50 mm Hg (III)	0.40	0.16	20 (25)	0.21 (0.19)	1.02 (0.89)	1.04 (0.91)
30 mm Hg (IV)	0.69	0.30	18 (25)	0.31 (0.25)	0.87 (0.70)	0.90 (0.73)
Mild hypoxemia (N = 5) (*Hudetz et al, 1997*)						
Control (0)	0.95	0.36	25	0.30	1.00	1.00
40 mm Hg (I)	0.72	0.31	23 (25)	0.28 (0.26)	0.92 (0.89)	0.92 (0.92)
Severe hypoxemia (N = 5) (*Krolo and Hudetz, 2000*)						
Control (0)	1.41	1.20	25	0.31	1.00	1.00
26 mm Hg (I)	0.87	0.63	20 (25)	0.31 (0.26)	0.85 (0.69)	0.63 (0.50)
Mild hypercapnia (N = 6) (*Villringer et al, 1994*)						
33 mm Hg (0)	1.29	1.02	25	0.31	1.00	1.00
50 mm Hg (I)	0.82	0.76	27 (25)	0.22 (0.24)	1.14 (1.23)	1.02 (1.10)
Severe hypercapnia (N = 10) (*Hudetz et al, 1997*)						
35 mm Hg (0)	0.91	0.97	25	0.24	1.00	1.00
67 mm Hg (I; $N = 5$)	0.61	0.75	28 (25)	0.17 (0.19)	1.04 (1.16)	0.91 (1.02)
97 mm Hg (II; $N = 5$)	0.64	0.72	30 (25)	0.17 (0.20)	0.99 (1.19)	0.84 (1.02)

OEF^{max}, maximum oxygen extraction fraction; $CMRO_2^{max}$, maximum metabolic rate of oxygen; CTTH, capillary transit time heterogeneity; RBC, red blood cell. Also given are estimates of tissue oxygen tension, required by the model (see Materials and methods). To illustrate the independent roles of CTTH and tissue oxygen tension changes during physiological stimuli, oxygen availability values, calculated under the assumption that these model variables remain constant, are also reported in the Table. Physiological conditions were assigned symbols (see legend, Figure 4) and roman numerals to allow identification in Figure 4.

In the homogenous case with $f_1 = f_2$ and net flow $F_{het} = f_1 + f_2$, the net oxygen extraction is illustrated by the full red line in Figure 2B. If we now maintain net flow, but let f_1 decrease and f_2 increases, the decreasing slope of the flow—$CMRO_2^{max}$ relation towards high flow causes the loss of net oxygen extraction from the first population (with lower flow f_1) to *always be larger* than the gain from the second population (with higher flow f_2). It follows from this property that although *CBF* increases, net oxygen extraction may in principle still decrease: In Figure 2B, this is illustrated by comparing the net oxygen extraction in the latter case (two flow populations with $f_1 < f_2$) with a homogenous case (with flow F_{hom}). As indicated by the double asterisk, net oxygen extraction is smaller in the heterogeneous case, albeit $F_{het} > F_{hom}$. While these examples illustrate that the intuitive, increasing *CBF*–$CMRO_2^{max}$ relation is lost due to the parallel organization of exchange vessels in biological tissues, they also suggest that this paradoxical behavior may be more likely to occur if capillary flows cannot be homogenized in response to increases in flow. (Note that the phenomenon may also occur if the lower flow state displays a narrow distribution of flow values).

In the absence of recruitment, capillary transit time heterogeneity affects maximum oxygen extraction fraction for a given cerebral blood flow: Using again the Crone-Renkin expression, Figure 3 shows arteriolar, capillary, and venular oxygen concentrations for a transit time distribution measured in resting rat brain (Figure 3A) by Stefanovic *et al* (2008). The actual transit times represented in Figure 3A were generated by sampling a gamma distributions with parameters found by matching mean and standard

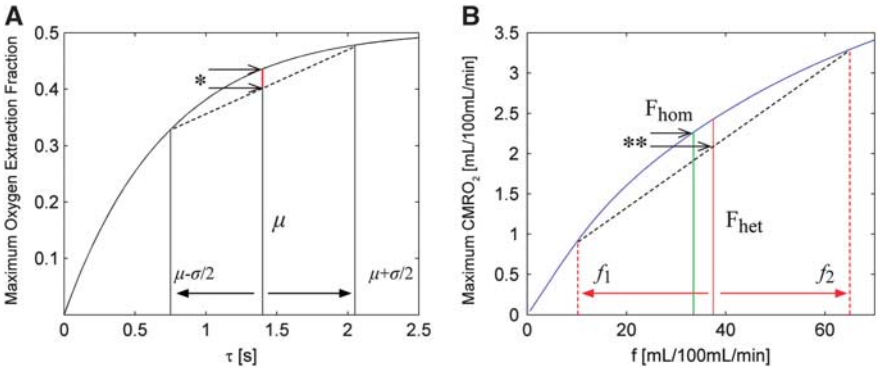

Figure 2 Oxygen extraction as a function of capillary transit time. (**A**) The maximum attainable oxygen extraction fraction versus transit time is shown. Note that oxygen extraction becomes inefficient toward short mean transit times, $\mu = CBV'/CBF$. The same principle applies to individual transit times along separate paths in the capillary tree. However, the effect is nonlinear, and because of the concave nature of the curve, a broad capillary transit time distribution (illustrated here by two populations with transit times $\mu-\sigma/2$ and $\mu+\sigma/2$) yields considerably lower OEF^{max} (indicated by the asterisk) for this distribution than the corresponding *homogenous* distribution, where all capillary transits have identical transit time μ. The same phenomenon may result in a decreased net oxygen extraction despite an increased net flow: in (**B**), maximum $CMRO_2$ is plotted versus flow using our model, and here the green line indicates the flow and associated $CMRO_2^{max}$ from a homogeneous population of capillaries with a net flow F_{hom}. A slightly larger flow $F_{het} > F_{hom}$, indicated by the red line is now accommodated by the same capillary bed, but divided into two populations, where one population has flow f_1 and the other f_2, $f_1 + f_2 = F_{het}$. However, the net oxygen extraction in this case (intersection of the dashed diagonal line with the red vertical line) is in fact smaller than that obtained for the homogenous, lower flow case, as indicated by the double asterisk. CBF, cerebral blood flow; CBV', capillary blood volume; OEF^{max}, maximum oxygen extraction fraction; $CMRO_2$, cerebral metabolic rate of oxygen; $CMRO_2^{max}$, maximum $CMRO_2$.

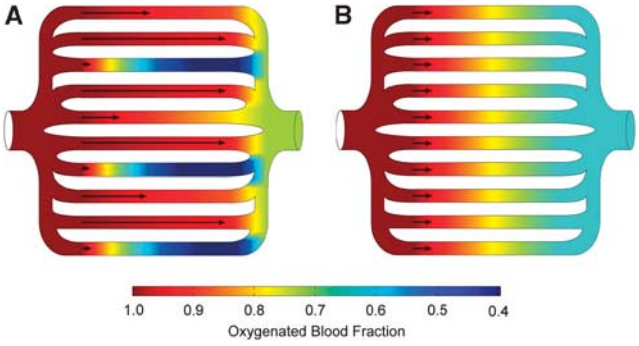

Figure 3 Effects of capillary transit time heterogeneity (CTTH) on oxygen extraction. (**A**, **B**) Compare the extraction of oxygen from individual capillaries according to commonly accepted Crone-Renkin kinetics when the same flow is distributed across the same number of parallel capillary paths with homogenous (**B**) capillary flow velocities (arrows), and heterogeneous flow velocities (**A**), respectively. Transit times in the resting, heterogeneous case were obtained by sampling a gamma distribution with parameters corresponding to recordings of mean and standard deviation of transit times in a rat (Stefanovic *et al*, 2008). Notice that venous outflow oxygen concentration is affected by the heterogeneity of capillary flows, in spite of identical total blood flows and number of open capillaries.

deviation to the measurements by Stefanovic and colleagues (Stefanovic *et al*, 2008). Also shown is the case of identical μ (and thus CBF), but homogenous capillary transit times (Figure 3B), which corresponds to our current notion of purely 'arteriolar' regulation of oxygen delivery, and a single capillary transit time. In the resting state, poor oxygen extraction efficiency in capillaries with short transit times dominates over the slightly better extraction in vessels with transit times longer than the mean (as evidenced by the higher venular-end capillary oxygenation), reducing net oxygen extraction capacity compared with the 'homogenous' case. Importantly, this example shows theoretically that tissue oxygenation can increase in the absence of traditional recruitment (opening of previously closed capillaries) and *CBF* changes, solely by modulating CTTH.

Quantitative Analysis

Combined effect of capillary transit time heterogeneity and vasodilation on maximum oxygen extraction fraction: The model predicts that the hemodynamic contribution to tissue oxygenation is determined by RBC *mean* transit time μ, which by the Central Volume Theorem equals the CBV'/CBF ratio, and the *heterogeneity* of RBC transit times, CTTH, quantified here as the standard deviation of capillary RBC transit times, σ. While these quantities can readily be observed by dynamic *in-vivo* microscopy studies, they also conveniently separate the oxygenation effect of tissue hemodynamics into a 'conventional', macroscopic term, controlled by arterial and arteriolar diameter, namely the CBV'/CBF ratio, and the new term σ, which depends on the microscopic distribution of RBCs. In the following, we will maintain μ as the x axis while reporting the ways in which σ and interstitial oxygen tension affect tissue oxygenation.

Figure 4A shows the combined contour and intensity plot of OEF^{max} as a function of μ and σ. In agreement with the findings above, OEF^{max} varies greatly for given *CBF* and *CBV′* (and hence μ) values, according to the 'microscopic' term σ. Note that for a fixed μ, the most efficient oxygen extraction occurs for an infinitely narrow transit time distribution ($\sigma = 0$).

Combined effect of capillary transit time heterogeneity and vasodilation on maximum cerebral metabolic rate of oxygen: Figures 4B and 4C depict the maximum $CMRO_2$ that may be supported by the bloodstream, $CMRO_2^{max}$, based on the μ–OEF^{max} relation in Figure 4A. To express *CBF* in terms of μ in the expression $CMRO_2^{max} = CBF \cdot C_A \cdot OEF^{max}$, the central volume theorem $\mu = CBV'/CBF$ was applied, assuming (1) a constant *CBV′* (see Materials and methods), equal to the capillary volume fraction in Figure 4B, and (2) increasing *CBV′* as a function of CBF, according to Grubb's relation (Grubb *et al*, 1974), shown in Figure 4C. Note that the most efficient oxygen extraction again occurs for a homogeneous transit time distribution ($\sigma = 0$).

Malignant capillary transit time heterogeneity: In terms of tissue oxygenation, the effect of increased *CBF*—and thereby the supply of oxygenated blood—competes with the inherent reduction of extraction efficacy (OEF^{max}) that follows the parallel reduction in transit time (cf. Figure 2). While the classical assumption of $\sigma = 0$ implies that $CMRO_2^{max}$ always increases as a function of *CBF*, CTTH ($\sigma > 0$) effectively reduces OEF^{max} to cause an intriguing phenomenon as noted in Figure 4B and to a lesser extent in Figure 4C: the effects of hyperemia (reduction of transit time) on $CMRO_2^{max}$ differ according to the two phases separated by the yellow line: In the 'high CTTH' phase to the left of the line, net oxygen availability *decreases* in states of shorter mean transit time, creating a paradox situation in which hyperemia would result in a new steady-state condition with *lower* oxygen availability. We will refer to this phenomenon (CTTH above the yellow line for a given μ and P_t) as *malignant CTTH* hereafter, and note that it constitutes predicted oxygen availability for a steady-state condition after

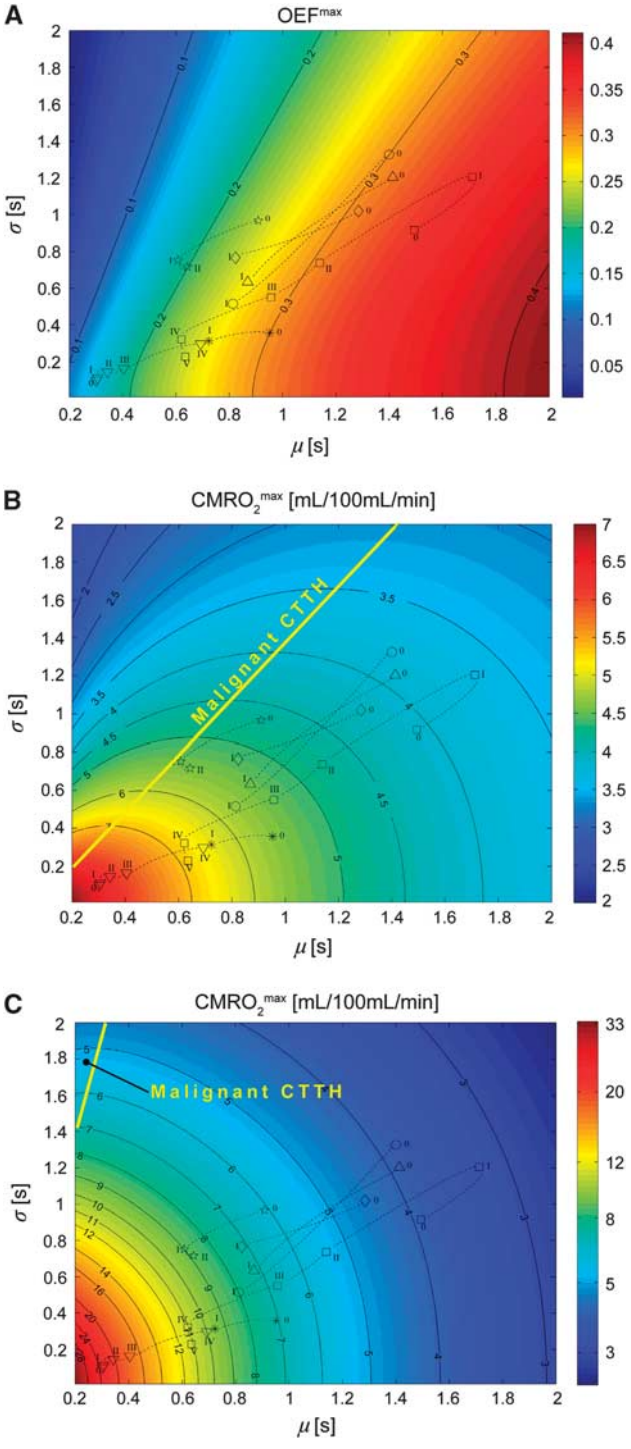

Figure 4 General model of the effects of transit time and capillary transit time heterogeneity (CTTH) on maximum oxygen extraction. Contour plot of maximum oxygen extraction fraction (OEF^{max}) (**A**) for a given mean transit time (μ) and capillary flow heterogeneity (σ). The corresponding maximum oxygen delivery is shown in (**B**) assuming fixed cerebral blood volume (*CBV′*) = 1.6%, and Grubb's relation (Grubb *et al*, 1974) in (**C**). Resting state values were assumed to be cerebral blood flow (*CBF*) = 60 mL/100 mL per minute and C_aO_2 = 19 mL/100 mL. Note that maximum oxygen delivery increases with decreasing flow heterogeneity. The yellow line in (**B**) separates states in which *shorter* transit times lead to *decreased* oxygen availability (dubbed malignant CTTH) from states where decreasing transit times lead to increased oxygen availability. Also shown are (μ,σ) values obtained in a range of physiological conditions—the symbols below refer to conditions listed in Table 1. The roman numeral accompanying each symbol allows identification of the corresponding physiological data in Table 1. Symbols: ○ = functional activation (Stefanovic *et al*, 2008); □ = cortical electrical stimulation (Schulte *et al*, 2003); ▽ = hypotension (Hudetz *et al*, 1995); ☆ = mild hypoxia (Hudetz *et al*, 1997); Δ = severe hypoxia (Krolo and Hudetz, 2000); ◇ = mild hypocapnia (Villringer *et al*, 1994); * = severe hypercapnia (Hudetz *et al*, 1997).

isolated reduction of μ: in biological systems, a range of regulatory mechanisms may prevent transitions to steady states with negative oxygen yield—see Discussion of luxury perfusion and exhausted reserve capacity below. Figure 4C shows that the assumption of a considerable capillary blood volume increase with *CBF*, implies that malignant CTTH occurs only at very short μ, and at high σ.

Isolated effects of tissue oxygen tension and cerebral blood flow on maximum oxygen extraction fraction and maximum cerebral metabolic rate of oxygen: Figure 5A shows the quantitative changes in OEF^{max} that results from *isolated* changes in tissue oxygen tension (and hence higher blood-tissue concentration gradients), for example, as a result of increased oxygen utilization during neuronal activation, or during ischemia and hypoxia. We kept CTTH constant at $\sigma = 1.3$ and *CBV′* at 1.6%. For steady-state conditions with short transit times (high *CBF*), oxygen tension has little effect on OEF^{max} and $CMRO_2^{max}$, as the inherent, poor extraction (cf. Figure 2) is only improved marginally by the higher oxygen concentration gradient. At long transit times, the effects of low tissue oxygen tension on OEF^{max} are substantial, as OEF^{max} isocontours become more horizontal, and P_t reductions therefore yield higher OEF^{max}. The resulting, net oxygenation $CMRO_2^{max}$ is shown in Figure 5B. For long transit times, the benefits of these higher OEF^{max} values are gradually outweighed by the lower *CBF*.

Oxygenation when cerebral blood flow cannot increase: critical thresholds: In conditions where *CBF* either cannot increase or is reduced, the model predicts that both reductions in tissue oxygen tension (owing to residual tissue metabolism) and reductions in CTTH may increase OEF^{max} to such an extent that oxygen availability may be preserved even during a substantial *CBF* reduction (and hence MTT increase)—see Figure 6. As a more fundamental physiological constraint, however, the models' equation (5) predicts that for mean transit times beyond 6 seconds, OEF^{max} becomes 99% of its maximal value (using $P_t = 25$ mm Hg, $\sigma = 0$ and $k = 118$ per second).

In-vivo data: relative roles of capillary transit time heterogeneity, cerebral blood flow, and oxygen tension: Table 1 shows data from all available *in-vivo* recordings, in which transit time characteristics were reported in such a manner that our model could be applied with limited assumptions, alongside realistic tissue oxygen tension values. Note that CTTH is large (σ relative to μ) in the control states of all

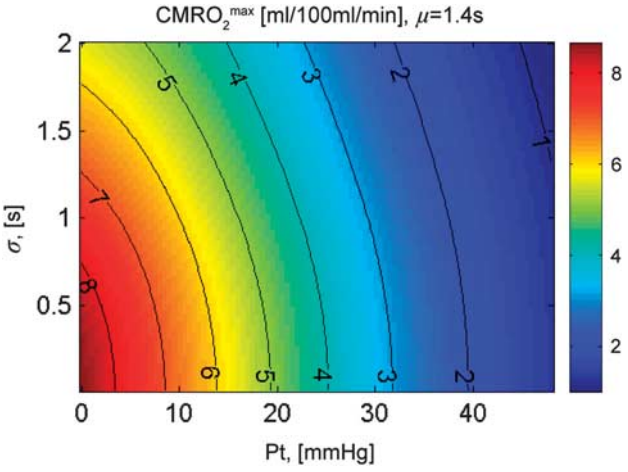

Figure 6 Net oxygen availability as a function of tissue oxygen tension and CTTH for fixed *CBF*. In this figure, *CBF* and *CBV′* were kept constant (*CBF* = 60 mL/100 mL per minute; *CBV′* = 1.6%; mean transit time $\mu = 1.4$ seconds) to illustrate how tissue oxygen tension and CTTH contribute to the metabolic needs of tissue during rest and as metabolic needs are increased with blocked *CBF*. Note that observed oxygen tension increases of 5% typically support $CMRO_2$ increases of 25%. CTTH, capillary transit time heterogeneity; OEF^{max}, maximum oxygen extraction fraction; CBF, cerebral blood flow; CBV, cerebral blood volume; $CMRO_2$, cerebral metabolic rate of oxygen.

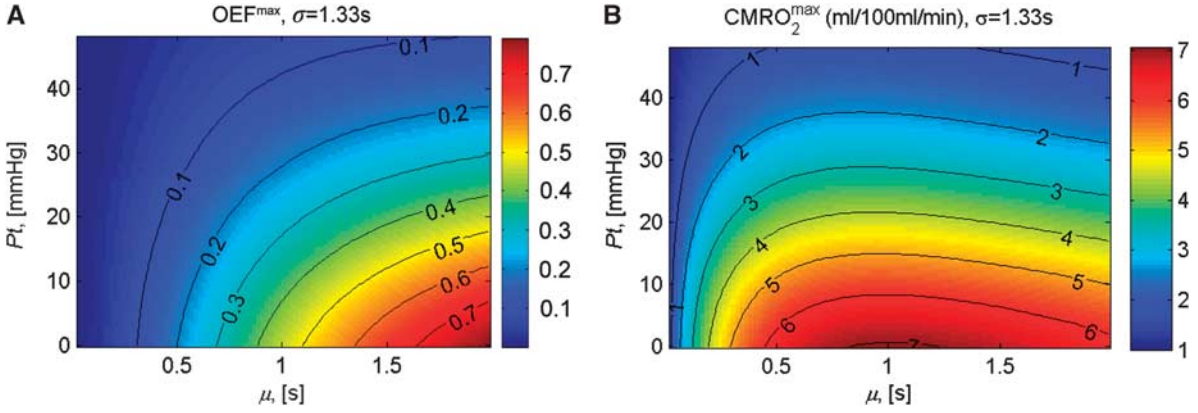

Figure 5 Maximum oxygen extraction fraction and maximum oxygen utilization for fixed CTTH. This figure illustrates the biophysical effects of reduced oxygen tension (as a result of tissue oxygen utilization) in the case of fixed CTTH ($\sigma = 1.33$ seconds). A reduction in tissue oxygen tension can seemingly maintain high OEF^{max} (**A**) and thus $CMRO_2^{max}$, except toward short mean transit times (high *CBF*). Values as in Figure 4. CTTH, capillary transit time heterogeneity; OEF^{max}, maximum oxygen extraction fraction; CBF, cerebral blood flow; $CMRO_2^{max}$, maximum cerebral metabolic rate of oxygen.

studies, emphasizing the importance of incorporating CTTH in models of oxygen transport. The μ and σ values determined in the various physiological states are illustrated in the OEF^{max} and $CMRO_2^{max}$ contour plots in Figure 4 (symbols and roman numerals in Figure 4 correspond to the corresponding physiological conditions and roman numerals in Table 1). In Table 1, the relative importance of CTTH changes during physiological challenges is determined by calculating the maximum attainable $CMRO_2$ with and without (i.e., driven solely by *CBF* and tissue oxygen tension changes) the reported CTTH changes (rightmost column). Also, oxygenation changes with and without parallel tissue oxygen tension changes are reported.

Tissue oxygenation during functional activation and cortical electrical stimulation: Qualitative observations of RBC or plasma flows during functional activation consistently report CTTH reductions during functional hyperemia (Vogel and Kuschinsky, 1996), with capillaries showing low velocities during rest also being those who display the largest velocity increases during activation (Stefanovic *et al*, 2008). In direct *cortical electrical stimulation* (Schulte *et al*, 2003), data showed (except for one data point), gradual reduction of CTTH and OEF^{max} with increase in current strength, resulting in increasing maximum oxygen utilization rates. This concurs with expected metabolic needs, as increased electrode current (as opposed to frequency) is believed to elicit firing of an increasing number of neurons in the rat cortex (Schulte *et al*, 2003). $CMRO_2$ increases recorded by magnetic resonance imaging and positron emission tomography in humans in relation to sensory stimulation are typically at the order of 15% to 20% depending on method, and stimulus type and intensity, while reported changes in anesthetized animals are generally considerably larger (Lin *et al*, 2010; Shulman *et al*, 2002). The two rightmost columns in Table 1 show that—given the parallel functional hyperemia and increased tissue oxygen tension—CTTH reduction is necessary to explain increased oxygen availability during functional activation and maximal cortical electrical stimulation. Without this transit time homogenization, the tissue oxygen tension would seemingly need to be unaffected during the 2- to 3-fold *CBF* increase to support a 5% increase in oxygenation for functional activation, and 21% for cortical electrical stimulation.

To test whether a *CBF* increase is necessary to support neuronal activation, we revisit Figure 6, which shows the combined effect of CTTH reduction and an oxygen tension drop driven by tissue oxidative metabolism at constant *CBF* and *CBV*′. We note that oxygen tension drops (5 mm Hg) recorded during functional activation with blocked *CBF* response (Masamoto *et al*, 2009) with typical CTTH reductions reported during neuronal activation (Table 1) seemingly support a 25% increase in $CMRO_2$, in agreement with findings of preserved neuronal firing despite blocked *CBF* (Leithner *et al*, 2010; Masamoto *et al*, 2009).

Tissue oxygenation during cerebral hypotension: In *hemorrhagic hypotension*, CTTH seemingly plays a lesser role than tissue oxygen tension in maintaining oxygen delivery as perfusion pressure drops (Table 1). Note that CTTH *increased* with gradual loss of perfusion pressure (autoregulation in terms of RBC flux was lost as cerebral perfusion pressure dropped below 75 mm Hg), rapidly diminishing the contribution from CTTH to total oxygen delivery in this animal model.

Tissue oxygenation during hypoxia: In *hypoxia*, transit time homogenization was observed as arterial oxygen tension decreased, resulting in high OEF^{max} despite dramatic increases in *CBF*. Our model hence predicts that oxygen availability was preserved during severe hypoxia, which could be equally attributed to CTTH reduction and vasodilation (Table 1). In this case, CTTH reductions were clearly necessary to maintain resting metabolism.

Tissue oxygenation in hypercapnia: In *hypercapnia,* the combined studies of Villringer *et al* (1994) and Hudetz *et al* (1997) showed reduction of CTTH in proportion to the increase in $PaCO_2$, in agreement with a qualitative study by Abounader *et al* (1995) in conscious rats. Interestingly, the model predicted largely unaltered oxygenation, despite a large increase of flow during CO_2 inhalation (Villringer *et al*, 1994; Hudetz *et al*, 1997), as hemodynamic changes seemingly adapt oxygen delivery to the expected, unaltered metabolic needs. We note that the hemodynamic changes resembled those of somatosensory and cortical stimulation, as commonly assumed in studies of the neurovascular coupling.

Summary of findings: The CTTH reduction is seemingly important to counteract OEF^{max} reductions during hyperemia, while reduced tissue oxygen tension seems important to drive normal oxygen metabolism during hypoperfusion. Of note, this conclusion did not depend on the assumed, resting tissue oxygen tension (results not shown). Our results are consistent with close coupling between cerebral hemodynamics and metabolism across a wide range of *CBF* values and physiological states, albeit neurovascular coupling is achieved by the combined effects of *CBF* and CTTH changes.

Discussion

The model developed here extends existing models of oxygen extraction in brain to include the effects of tissue oxygen tension and CTTH, based on oxygen tension measurements and RBC transit time recordings readily available from *in-vivo* micro-

scopy studies or the mean and standard deviations of 3D RBC velocity distributions recorded by Laser-Doppler Flowmetry. Using accepted diffusion properties of single capillaries, our model shows that it is a basic property of the parallel organization of capillaries that oxygen extraction capacity depends not only on tissue oxygen tension, and arterial and arteriolar tone (as quantified by *CBV′* and *CBF*; the mean transit time, the *x* axis in Figure 4), but also to a large extent on the distribution of capillary transit times (as quantified by the standard deviation of capillary transit times, the *y* axis in Figure 4). This finding is in qualitative agreement with modeling and experimental studies of oxygen metabolism in heart (Cousineau *et al*, 1983) and in muscle (Kalliokoski *et al*, 2004).

The model thereby extends the original notion of capillary recruitment by showing that this phenomenon represents merely an extreme case of CTTH, while changes in CTTH alone (with all capillaries open) may alter the effective capillary surface area available for diffusion several-fold. We note that the apparent permeability-surface area product may be determined from OEF^{max} using the expression $PS = -CBF \ln(1-OEF^{max})$.

Direct observations of the capillary bed in rat brain during rest consistently show RBC transit times to be extremely heterogeneous, constantly varying along and among capillary paths (Villringer *et al*, 1994; Pawlik *et al*, 1981; Kleinfeld *et al*, 1998) with transit time standard deviations ranging from 30% to 100% of the mean transit time (see Table 1). Based on these *in-vivo* results, our analysis clearly shows that it is crucial to include the effects of CTTH in studies of the coupling between cerebral oxygen metabolism and local hemodynamics. Model analysis of these data hence confirms the effects of CTTH on brain oxygenation as hypothesized by Kuschinsky and Paulson (1992).

A crucial, physiological effect of CTTH reductions is seemingly to counteract the drop in OEF (Figure 4A) that invariably occurs during hyperemia. This property has indeed been demonstrated in heart (Cousineau *et al*, 1983) and in muscle (Kalliokoski *et al*, 2004). In cerebral *hypo*perfusion, the model predicts that the resulting, lower tissue oxygen tension increases OEF^{max}, thereby facilitating the maintenance of resting oxygen supply down to cerebral perfusion pressure levels below that of normal autoregulation (Hudetz *et al*, 1995)—under the assumption that CTTH is unaltered by the lower perfusion. In the study by Hudetz *et al* (1995), however, decreased cerebral perfusion pressure, led to parallel *increases* in μ and σ, effectively reducing tissue oxygenation (see Figure 4B). Increased capillary flow heterogeneity was also reported by Tomita *et al* (2002) in a model of ischemic stroke, suggesting that CTTH increase may be a crucial phenomenon which reduces oxygenation in ischemia, in a manner that may not be detected by *CBF* changes alone. The *malignant CTTH* phenomenon implies that such microvascular failure may have profound effects on tissue oxygen availability: Aside from a reduction of per-ischemic oxygenation, vessel recanalization may have paradoxical consequences if CTTH is not normalized. As *CBF* is restored and μ therefore becomes shorter, persisting, high σ values could result in a state of malignant CTTH (Figure 4B). We note that, in a biological system, the ensuing hypoxia/acidosis could stimulate upstream vasodilation and—in the absence of any inhibition—cause further *CBF* increase, and a new steady state with even lower oxygen availability; a vicious cycle which, if it occurs, could resemble the *luxury perfusion syndrome* (Lassen, 1966) which is observed across many tissue types on reperfusion. It should be noted that such decreased oxygen availability on vasodilatory signaling could be self-limiting due to a range of mechanisms, such as steeper oxygen gradients and lower NO availability due to substrate depletion (Attwell *et al*, 2010). In biological systems, malignant CTTH may therefore manifest itself as a blunted *CBF* response (exhausted cerebrovascular reserve capacity) rather than 'uncontrolled' hyperemia.

Capillary Transit Time Heterogeneity During Rest and Physiological Stimuli

The extent to which CTTH reduction in response to physiological stimuli is an actively regulated mechanism, or a passive effect of increased RBC flux and altered pressure distributions in a complex system of interconnected microvessels, remains poorly understood. The studies analyzed here, and findings in heart and muscle (Cousineau *et al*, 1983; Kalliokoski *et al*, 2004), generally show decreasing CTTH as a function of flow. The notion of a passive process, however, is contradicted by findings of *reduced* CTTH in hypocapnic rats (Vogel *et al*, 1996), where *CBF* is significantly reduced, and in some cases of acute human stroke (Østergaard *et al*, 2000).

Active regulation of capillary perfusion patterns has been speculated to arise from redistribution of capillary flows by means of precapillary sphincters and functional thoroughfare channels (Hudetz *et al*, 1996), or by contractile, capillary pericytes, found on the albuminal side of endothelial cells. Peppiatt and colleagues demonstrated that a proportion of cerebellar pericytes dilate in response to local electrical stimulation and GABAergic and glutamatergic signaling, suggesting a link between local inhibitory/excitatory signaling and capillary hemodynamics. In a recent paper, Fernandez-Klett *et al* (2010) showed that pericytes control capillary diameter *in vivo*, while arterioles elicit hyperemia in their experimental setting. While this contradicted the notion that pericytes elicit upstream vasodilation (Peppiatt *et al*, 2006; Attwell *et al*, 2010), we speculate that such pericyte action could still have profound metabolic implications, as generalized pericyte dilation would

permit more homogenous flow of RBCs in response to local release of neurotransmitters, facilitating higher OEF. The analysis of RBC velocity data in Table 1 suggests that the *combined* effect of changes in CTTH and *CBF* on tissue oxygen availability is in better agreement with hemodynamic-metabolism coupling than the effect of *CBF* changes taken alone. Pericytes could, therefore, be part of a *neurocapillary* coupling mechanism, by modulating OEF^{max}, rather than *CBF*. It should be kept in mind, however, that the heterogeneity of RBC capillary transit times depends on the topology and morphology of the entire microvascular network (Pries *et al*, 1996). Therefore, the diameter or pressure response recorded in single capillaries cannot necessarily be generalized to predict overall hemodynamic changes (Pries *et al*, 1995). For example, *constriction* of functional thoroughfare channels with subsequent redistribution of RBCs to capillaries with more homogenous transit times would, according to our findings, result in far more efficient oxygen extraction.

Cerebral Blood Flow–Maximum Cerebral Metabolic Rate of Oxygen Relation and Malignant Capillary Transit Time Heterogeneity: Effects of the Assumed Cerebral Blood Flow–Capillary Blood Volume Relation

The model quantifies OEF^{max} based solely on P_t and the transit time characteristics of RBCs through the capillary bed, and is thus directly applicable to *in-vivo* microscopy recordings of capillary RBC transits. The further step of determining $CMRO_2^{max}$ as a function of μ, however, requires knowledge of the *CBF–CBV′* relation of oxygen exchanging vessels in the tissue in question. As seen by comparing Figures 4B and C, the physiological conditions under which malignant CTTH phenomenon exists clearly depends on this assumption, as use of the Grubb's relation (Figure 4C), which is based on observations of whole brain *CBF* and *CBV* (Grubb *et al*, 1974), lead to limited increase in $CMRO_2^{max}$ with hyperemia (decreasing μ), but only to malignant CTTH at very short μ in combination with large σ. The Grubb's relation implies that hyperemia leads to substantial increases in capillary volume (and thereby modest reductions in RBC transit time) during hyperemia. Direct observations of single RBCs during hypercapnia and functional activation show that RBC flux and velocity change in parallel during hyperemia (Villringer *et al*, 1994; Kleinfeld *et al*, 1998), and hence that transit times are inversely proportional to *CBF*, supporting the assumption of a constant capillary *CBV′*. Capillary *CBV* changes during hyperemia have undergone intense scrutiny: the redistribution of capillary flows to a more homogenous pattern during hyperemia is seemingly paralleled by a more homogenous distribution of capillary diameters, and an overall, small increase in capillary blood volume (Stefanovic *et al*, 2008), and in some studies an increased linear density of RBCs (Schulte *et al*, 2003). Relative capillary volume changes during hyperemia are, by conservative estimates, only half of the blood volume change predicted by the Grubb's relation (Stefanovic *et al*, 2008). While favored by hemodynamic data and predicted by our model, the existence of malignant CTTH clearly awaits experimental verification. In experimental studies, it should be kept in mind that capillary rarefaction and angiogenesis may effectively change *CBV′* and thus $CMRO_2^{max}$ for a given tissue volume, and experimental determination of (μ, σ) characteristics should thus be combined with estimates of density of oxygen exchanging vessels for reference.

Capillary Morphology and Capillary Transit Time Heterogeneity in Disease

As argued above, the maintenance of low CTTH seems important to maintain high *OEF* during hypoxic or ischemic episodes and during functional hyperemia. It, therefore, appears important to investigate whether early changes in capillary morphology in, for example, aging, hypertension, diabetes, stroke and Alzheimer's disease affect resting CTTH values, and thus the tissue oxygen tension and *CBF* values required for neuronal activity. While our model shows that the sensitivity of OEF^{max} to CTTH is a general property of the parallel organization of capillaries, it remains to be determined whether capillary flow patterns are disturbed to such an extent that the resulting OEF^{max} decrease affects the observed flow-metabolism coupling in these diseases. This could provide intriguing insight into the role of altered capillary flow patterns—in addition to those of large vessels—in the exhausted cerebrovascular reactivity in these conditions (Girouard and Iadecola, 2006).

Study Limitations

We assumed a very simple system of parallel, noncommunicating, equal-length capillary paths to capture the physiological implications of CTTH. In reality, intracortical capillaries show a relatively narrow distribution of segment lengths, but are highly tortuous, interconnected, and display a complex 3-dimensional arrangement that display considerable variability among brain regions, but no apparent symmetries (Pawlik *et al*, 1981). Moreover, the distributions of flow and hematocrit across such capillary networks have been shown to be highly complex functions of their morphology and topology (Pries *et al*, 1996). Adding to this complexity, it has been suggested that pericytes control the distribution of RBCs at capillary bifurcations and constantly adapt local capillary diameter according to local cellular needs (Yamanishi *et al*, 2006), possibly adding to observed, rapid variations in oxygen tension at the distance scale of typical intercapillary distances (25 to 40 μm), at a time scale

of the passage of single RBCs and rapidly changing energy requirements of surrounding cells (Ndubuizu and LaManna, 2007). We, therefore, chose an approach based on observable properties of RBC transit time characteristics rather than capillary network topology and morphology in modeling blood-tissue oxygen transport.

While the system characteristics seemingly preclude attempts to characterize (and much less to model) spatial oxygen tensions and the oxygen flux from capillaries to individual cells, capillary morphology and topology itself is seemingly the result of oxygen tension-sensitive mechanisms (mediated by pericytes, who are essential during developmental and adaptive angiogenesis) that match local capillary density to cellular demands (Dore-Duffy and LaManna, 2007). In the normal brain, these mechanisms may favor a relative uniformity of local transit time characteristics and time-averaged tissue oxygen tension. We hence assumed a constant value of the oxygen tension in tissue immediately outside the capillaries, in line with the recently suggested 'revised oxygen limitation hypothesis', according to which blood supply is regulated so as to maintain a constant, nonvanishing oxygen tension (Buxton, 2010). We believe that rapid variations in oxygen tension have little effects on the predictions of our model, including the malignant CTTH phenomenon, in terms of the implications of capillary flow heterogeneity. The model findings suggest, however, that changes in oxygen tension gradients in tissue represent an additional means of regulating oxygen supply, for example, in hypoperfusion.

It should be emphasized that the model predicts the relationships between the variables OEF^{max}, C_t, μ, and σ in steady state only. In terms of applying the model, this means that the tissue concentration of oxygen should not change appreciably, compared with the arterial-venous oxygen difference, during a typical mean transit time. In particular, the model cannot predict dynamic responses of the variables C_t, μ, and σ if one of these variables is perturbed by a physiological challenge. For example (as discussed above), a vasodilatory signal in a malignant CTTH condition could result in either dysregulated hyperperfusion or largely unaltered *CBF* (exhausted reserve capacity) in which tissue oxygenation is instead driven by lower oxygen tension. The study of such dynamic changes requires further measurements or assumptions to apply the model.

Cerebral capillaries display a distribution of lengths, and are interconnected, such that the model in Figure 1 is somewhat oversimplified. Capillary transit time distributions, therefore, reflect the underlying distribution of capillary lengths, as well as the velocity distribution of RBCs. Also, capillary branching, with interconnections to other capillaries, tends to equilibrate oxygen tensions across parallel capillary paths. These aspects mostly affect the estimation of absolute transit time heterogeneities from literature data that report these in terms of blood flow, RBC velocities, or cell fluxes, but do not reduce the quantitative effects of CTTH changes reported here.

A fundamental assumption in our model was that oxygen transfer across the capillary wall is proportional to the difference in concentration, and given the substantial challenges associated with measuring oxygen tension and its solubility in tissue *in vivo*, we assumed similar solubilities of oxygen in plasma and in tissue for simplicity. An extension to the model would incorporate, for example, differences in chemical affinity in the two compartments including nonlinear oxygen binding to neuroglobin in the parenchyma. Considering these and additional factors that affect oxygen binding to hemoglobin, such as pH (the Bohr effect), could improve our model (e.g., the analysis of oxygen binding under increased CO_2 levels), but would not change the overall conclusions of the study. Oxygen kinetics was described in terms of two compartments (three including hemoglobin) with a single rate constant related to the capillary membranes' permeability to oxygen. If oxygen is well stirred in the capillary and tissue, then the nonspatial description provided by a compartmental model with a single characteristic timescale is accurate. We assumed a gamma variate distribution of transit times through the capillary bed. This assumption is accepted in the modeling of capillary transit time dynamics (King *et al*, 1996), and convenient for the analytical mathematical approach chosen here. Other distributions could equally have been used, but the overall conclusions of our study are not believed to be very sensitive to the particular choice. Bassingthwaighte and colleagues have pioneered the development of advanced multiparameter models that allow detailed modeling of microvascular flow heterogeneity (albeit as a fixed proportion of local flow) (King *et al*, 1996; Østergaard *et al*, 1999), while also taking subsequent axial diffusion, tissue binding, and metabolism of oxygen (including the effects of metabolic CO_2 on pH) into account (Li *et al*, 1997; Dash and Bassingthwaighte, 2006). The analytical approach presented in this paper, however, has the benefits of capturing qualitative, physiological implications of CTTH based on only three parameters, allowing easy model overview and, in principle, direct applications of the model to transit time characteristics obtained by perfusion techniques (Mouridsen *et al*, 2011), or direct *in-vivo* observations (Kleinfeld *et al*, 1998; Stefanovic *et al*, 2008) of RBCs, using literature or directly measured tissue oxygen tensions.

Acknowledgements

The authors thank Professor David Attwell, UCL, London, and Professor Ulrich Dirnagl, Charité, Berlin, for helpful suggestions to our manuscript; Henriette Blæsild Vuust for artwork; and Chris Ørum for technical assistance.

Disclosure/conflict of interest

The authors declare no conflict of interest.

References

Abounader R, Vogel J, Kuschinsky W (1995) Patterns of capillary plasma perfusion in brains in conscious rats during normocapnia and hypercapnia. *Circ Res* 76:120–6

Attwell D, Buchan AM, Charpak S, Lauritzen M, Macvicar BA, Newman EA (2010) Glial and neuronal control of brain blood flow. *Nature* 468:232–43

Buxton RB (2010) Interpreting oxygenation-based neuroimaging signals: the importance and the challenge of understanding brain oxygen metabolism. *Front Neuroenergetics* 2:8

Buxton RB, Frank LR (1997) A model for the coupling between cerebral blood flow and oxygen metabolism during neural stimulation. *J Cereb Blood Flow Metab* 17:64–72

Buxton RB, Wong EC, Frank LR (1998) Dynamics of blood flow and oxygenation changes during brain activation: the balloon model. *Magn Reson Med* 39:855–64

Cousineau D, Rose CP, Lamoureux D, Goresky CA (1983) Changes in cardiac transcapillary exchange with metabolic coronary vasodilation in the intact dog. *Circ Res* 53:719–30

Crone C (1963) The permeability of capillaries in various organs as determined by use of the 'indicator diffusion' method. *Acta Physiol Scand* 58:292–305

Dash RK, Bassingthwaighte JB (2006) Simultaneous blood-tissue exchange of oxygen, carbon dioxide, bicarbonate, and hydrogen ion. *Ann Biomed Eng* 34:1129–48

Davis TL, Kwong KK, Weisskoff RM, Rosen BR (1998) Calibrated functional MRI: mapping the dynamics of oxidative metabolism. *Proc Natl Acad Sci USA* 95:1834–9

Derdeyn CP, Videen TO, Yundt KD, Fritsch SM, Carpenter DA, Grubb RL, Powers WJ (2002) Variability of cerebral blood volume and oxygen extraction: stages of cerebral haemodynamic impairment revisited. *Brain* 125: 595–607

Donahue MJ, Stevens RD, de Boorder M, Pekar JJ, Hendrikse J, van Zijl PC (2009) Hemodynamic changes after visual stimulation and breath holding provide evidence for an uncoupling of cerebral blood flow and volume from oxygen metabolism. *J Cereb Blood Flow Metab* 29:176–85

Dore-Duffy P, LaManna JC (2007) Physiologic angiodynamics in the brain. *Antioxid Redox Signal* 9:1363–71

Fernandez-Klett F, Offenhauser N, Dirnagl U, Priller J, Lindauer U (2010) Pericytes in capillaries are contractile *in vivo*, but arterioles mediate functional hyperemia in the mouse brain. *Proc Natl Acad Sci USA* 107:22290–5

Fox PT, Raichle ME (1986) Focal physiological uncoupling of cerebral blood flow and oxidative metabolism during somatosensory stimulation in human subjects. *Proc Natl Acad Sci USA* 83:1140–4

Girouard H, Iadecola C (2006) Neurovascular coupling in the normal brain and in hypertension, stroke, and Alzheimer disease. *J Appl Physiol* 100:328–35

Grubb Jr RL, Raichle ME, Eichling JO, Ter-Pogossian MM (1974) The effects of changes in $PaCO_2$ on cerebral blood volume, blood flow, and vascular mean transit time. *Stroke* 5:630–9

Hayashi T, Watabe H, Kudomi N, Kim KM, Enmi J, Hayashida K, Iida H (2003) A theoretical model of oxygen delivery and metabolism for physiologic interpretation of quantitative cerebral blood flow and metabolic rate of oxygen. *J Cereb Blood Flow Metab* 23:1314–23

Hudetz AG, Biswal BB, Feher G, Kampine JP (1997) Effects of hypoxia and hypercapnia on capillary flow velocity in the rat cerebral cortex. *Microvasc Res* 54:35–42

Hudetz AG, Feher G, Kampine JP (1996) Heterogeneous autoregulation of cerebrocortical capillary flow: evidence for functional thoroughfare channels? *Microvasc Res* 51:131–6

Hudetz AG, Feher G, Weigle CG, Knuese DE, Kampine JP (1995) Video microscopy of cerebrocortical capillary flow: response to hypotension and intracranial hypertension. *Am J Physiol* 268:H2202–10

Hyder F, Shulman RG, Rothman DL (1998) A model for the regulation of cerebral oxygen delivery. *J Appl Physiol* 85:554–64

Kalliokoski KK, Knuuti J, Nuutila P (2004) Blood transit time heterogeneity is associated to oxygen extraction in exercising human skeletal muscle. *Microvasc Res* 67:125–32

King RB, Raymond GM, Bassingthwaighte JB (1996) Modeling blood flow heterogeneity. *Ann Biomed Eng* 24:352–72

Kleinfeld D, Mitra PP, Helmchen F, Denk W (1998) Fluctuations and stimulus-induced changes in blood flow observed in individual capillaries in layers 2 through 4 of rat neocortex. *Proc Natl Acad Sci USA* 95:15741–6

Krogh A (1919) The supply of oxygen to the tissues and the regulation of the capillary circulation. *J Physiol (London)* 52:457–74

Krolo I, Hudetz AG (2000) Hypoxemia alters erythrocyte perfusion pattern in the cerebral capillary network. *Microvasc Res* 59:72–9

Kruger G, Kleinschmidt A, Frahm J (1996) Dynamic MRI sensitized to cerebral blood oxygenation and flow during sustained activation of human visual cortex. *Magn Reson Med* 35:797–800

Kuschinsky W, Paulson OB (1992) Capillary circulation in the brain. *Cerebrovasc Brain Metab Rev* 4:261–86

Lassen NA (1966) The luxury-perfusion syndrome and its possible relation to acute metabolic acidosis localised within the brain. *Lancet* 2:1113–5

Leithner C, Royl G, Offenhauser N, Fuchtemeier M, Kohl-Bareis M, Villringer A, Dirnagl U, Lindauer U (2010) Pharmacological uncoupling of activation induced increases in *CBF* and *CMRO2*. *J Cereb Blood Flow Metab* 30:311–22

Li Z, Yipintsoi T, Bassingthwaighte JB (1997) Nonlinear model for capillary-tissue oxygen transport and metabolism. *Ann Biomed Eng* 25:604–19

Lin AL, Fox PT, Hardies J, Duong TQ, Gao JH (2010) Nonlinear coupling between cerebral blood flow, oxygen consumption, and ATP production in human visual cortex. *Proc Natl Acad Sci USA* 107:8446–51

Malonek D, Dirnagl U, Lindauer U, Yamada K, Kanno I, Grinvald A (1997) Vascular imprints of neuronal activity: relationships between the dynamics of cortical blood flow, oxygenation, and volume changes following sensory stimulation. *Proc Natl Acad Sci USA* 94: 14826–31

Mandeville JB, Marota JJ, Ayata C, Zaharchuk G, Moskowitz MA, Rosen BR, Weisskoff RM (1999) Evidence of a cerebrovascular postarteriole windkessel

with delayed compliance. *J Cereb Blood Flow Metab* 19:679–89
Masamoto K, Vazquez A, Wang P, Kim SG (2009) Brain tissue oxygen consumption and supply induced by neural activation: determined under suppressed hemodynamic response conditions in the anesthetized rat cerebral cortex. *Adv Exp Med Biol* 645:287–92
Mintun MA, Lundstrom BN, Snyder AZ, Vlassenko AG, Shulman GL, Raichle ME (2001) Blood flow and oxygen delivery to human brain during functional activity: theoretical modeling and experimental data. *Proc Natl Acad Sci USA* 98:6859–64
Mouridsen K, Østergaard L, Christensen S, Jespersen SN (2011) Reliable estimation of capillary transit time distributions at voxel-level using DSC-MRI. In: *Proceedings of the International Society for Magnetic Resonance in Medicines 19th Annual Meeting and Exhibition*: 3915
Ndubuizu O, LaManna JC (2007) Brain tissue oxygen concentration measurements. *Antioxid Redox Signal* 9:1207–19
Østergaard L, Chesler DA, Weisskoff RM, Sorensen AG, Rosen BR (1999) Modeling cerebral blood flow and flow heterogeneity from magnetic resonance residue data. *J Cereb Blood Flow Metab* 19:690–9
Østergaard L, Sorensen AG, Chesler DA, Weisskoff RM, Koroshetz WJ, Wu O, Gyldensted C, Rosen BR (2000) Combined diffusion-weighted and perfusion-weighted flow heterogeneity magnetic resonance imaging in acute stroke. *Stroke* 31:1097–103
Pawlik G, Rackl A, Bing RJ (1981) Quantitative capillary topography and blood flow in the cerebral cortex of cats: an *in vivo* microscopic study. *Brain Res* 208:35–58
Peppiatt CM, Howarth C, Mobbs P, Attwell D (2006) Bidirectional control of CNS capillary diameter by pericytes. *Nature* 443:700–4
Pittman RN (2011) Oxygen gradients in the microcirculation. *Acta Physiol (Oxf)* 202:311–22
Pries AR, Secomb TW, Gaehtgens P (1995) Structure and hemodynamics of microvascular networks: heterogeneity and correlations. *Am J Physiol* 269:H1713–22
Pries AR, Secomb TW, Gaehtgens P (1996) Relationship between structural and hemodynamic heterogeneity in microvascular networks. *Am J Physiol* 270:H545–53
Roy CS, Sherrington CS (1890) On the regulation of the blood-supply of the brain. *J Physiol* 11:85–158.17
Schulte ML, Wood JD, Hudetz AG (2003) Cortical electrical stimulation alters erythrocyte perfusion pattern in the cerebral capillary network of the rat. *Brain Res* 963: 81–92
Shulman RG, Hyder F, Rothman DL (2002) Biophysical basis of brain activity: implications for neuroimaging. *Q Rev Biophys* 35:287–325
Stefanovic B, Hutchinson E, Yakovleva V, Schram V, Russell JT, Belluscio L, Koretsky AP, Silva AC (2008) Functional reactivity of cerebral capillaries. *J Cereb Blood Flow Metab* 28:961–72
Stewart GN (1894) Researches on the circulation time in organs and on the influences which affect it. Parts I–III. *J Physiol* 15:1–89
Tomita Y, Tomita M, Schiszler I, Amano T, Tanahashi N, Kobari M, Takeda H, Ohtomo M, Fukuuchi Y (2002) Moment analysis of microflow histogram in focal ischemic lesion to evaluate microvascular derangement after small pial arterial occlusion in rats. *J Cereb Blood Flow Metab* 22:663–9
Vafaee MS, Gjedde A (2000) Model of blood-brain transfer of oxygen explains nonlinear flow-metabolism coupling during stimulation of visual cortex. *J Cereb Blood Flow Metab* 20:747–54
Villringer A, Them A, Lindauer U, Einhaupl K, Dirnagl U (1994) Capillary perfusion of the rat brain cortex. An *in vivo* confocal microscopy study. *Circ Res* 75:55–62
Vimtrup B (1922) Beiträge zur Anatomie der Capillaren. I. Über contraktile Elemente in der Gefasswand der Blutkapillaren. *Zeitschr Anat Entwickl* 65:150–82
Vogel J, Abounader R, Schrock H, Zeller K, Duelli R, Kuschinsky W (1996) Parallel changes of blood flow and heterogeneity of capillary plasma perfusion in rat brains during hypocapnia. *Am J Physiol* 270:H1441–5
Vogel J, Kuschinsky W (1996) Decreased heterogeneity of capillary plasma flow in the rat whisker-barrel cortex during functional hyperemia. *J Cereb Blood Flow Metab* 16:1300–6
Yamanishi S, Katsumura K, Kobayashi T, Puro DG (2006) Extracellular lactate as a dynamic vasoactive signal in the rat retinal microvasculature. *Am J Physiol Heart Circ Physiol* 290:H925–34
Zheng Y, Martindale J, Johnston D, Jones M, Berwick J, Mayhew J (2002) A model of the hemodynamic response and oxygen delivery to brain. *Neuroimage* 16: 617–37